front, that is, in the afterburn region. The afterburn region is consistent with visual observation of the brightness of the burned sample being sustained for over 30 s and confirms an earlier report by Boldyrev *et al.* (*5*), who deduced the formation of two intermediates from their TR diffraction experiments in the second time regime.

It is clear from Fig. 3A that most of the observed scattering in the TR diffraction patterns was recorded in the 2θ region of 43° to 46°. In Fig. 4, the integrated intensity in this 2θ region is plotted as a function of time. This plot summarizes the TR diffraction events in the combusting Al-Ni system. It is characterized by a very sharp and high-intensity peak, peak A, at 5.4 s with a number of low-intensity peaks on either side. With decreased slit size, the number of these low-intensity peaks decreased as a result of a smaller number of grains correctly oriented to scatter the incident x-ray. This result lends credence to the effect of grain orientation or grain motion, or both, at high temperature on the multipeak features observed with the geometric resolution of our diffraction setup. After 20 s or so, broader peaks such as the one labeled B are observed. Beyond 50 s, the plot becomes almost featureless in accordance to a mere shift of the AlNi(110) product peak to high 2θ as a result of thermal contraction. Both features at A and B are reproducible in a number of Al + Ni samples repeatedly combusted under identical experimental conditions. Because grain orientation or random motions for individual grains at high temperature would not reproduce the same intensity peaks at the same time in successive scans, the sharp and high-intensity feature observed at 5.4 s is most likely due to an intermediate phase formed before the formation of the final AlNi product.

The technique of TR-XRD with synchrotron radiation is a very powerful and perhaps unique method for following phase transformations and chemical dynamics of solid combustion reactions in situ at high temperature. When temperature profile and wave-front velocity are measured synchronously and correlated with the TR diffraction scans, then all participating phases may be identified as a function of time and temperature. Intrinsic, real-time kinetic data of this sort are needed to allow critical testing of existing theoretical models of solid combustion and to provide the basis for developing new theories. In the case of the Al-Ni systems, there is a great interest in understanding the phase transformation and combustion dynamics as a function of the composition of the starting materials at various stoichiometric as well as off-stoichiometric compositions across the binary system (*27*). Finally, with brighter and higher flux synchrotron sources available currently at wiggler beamlines (~10^{12} photons per second) or next generation storage rings such as those of the Advanced Light Source (ALS) at Berkeley and the Advanced Photon Source (APS) at Argonne (10^{16} photons per second), higher spatial resolution should allow a "closer look" at the combustion front in this interesting class of high-temperature solid-state reactions.

REFERENCES AND NOTES

1. This is evident from the volume of articles published in *Combustion and Flame* since 1957.
2. Z. A. Munir, *Ceram. Bull.* **27**, 342 (1988).
3. P. Novikov, I. P. Borovinskaya, A. G. Merzhanov, in *Processes in Chemical Engineering and Metallurgy*, A. G. Merzhanov, Ed. (Chernogolovka, 1975), pp. 174–188.
4. Z. A. Munir and U. Anselmi-Tamburini, *Mater. Sci. Rep.* **3**, 277 (1989).
5. V. V. Boldyrev *et al.*, *Dok. Akad. Nauk SSSR* **259**, 1127 (1981).
6. A. G. Merzhanov, *Arch. Procesow Spalania* **5**, 17 (1974).
7. ———, *Arch. Combust.* **1**, 23 (1981).
8. S. M. Gruner, *Science* **238**, 305 (1987).
9. G. Zorn, E. Hellstern, H. Gobel, L. Schultz, *Adv. X-Ray Anal.* **30**, 483 (1987).
10. J. R. Schoonover and S. H. Lin, *J. Solid State Chem.* **76**, 143 (1988).
11. M. Sutton *et al.*, *Phys. Rev. Lett.* **62**, 288 (1988).
12. R. Clark and P. Hernandez, *ibid.*, p. 1768.
13. E. M. Larson, P. A. Waide, J. Wong, *Rev. Sci. Instrum.*, in press.
14. A. S. Rogachev, V. M. Shkiro, I. D. Chausskaya, M. V. Shvetsov, *Fiz. Goreniya Vzryva*, **24** (no. 6), 89 (1987).
15. Yu. S. Naiborodenko and V. I. Itin, *ibid.* **11**, 343 (1975).
16. ———, *ibid.*, p. 734.
17. E. A. Nekrasov, V. K. Smolyakov, Yu. M., Maksimov, *ibid.* **17**, 39 (1981).
18. A. G. Merzhanov *et al.*, *Poroshk. Metall.* **10**, 50 (1981).
19. K. A. Philpot, Z. A. Munir, J. B. Holt, *J. Mater. Sci.* **22**, 159 (1987).
20. J. B. Holt and Z. A. Munir, *ibid.* **21**, 151 (1986).
21. A. Bearden and A. F. Burr, *Rev. Mod. Phys.* **39**, 125 (1976).
22. N. F. Gmur, W. Thomlinson, S. M. White-DePace, *NSLS User's Manual: Guide to the VUV and X-ray Beamlines* (Brookhaven National Laboratory, Upton, NY, ed. 3, 1989).
23. S. D. Dunmead, D. W. Readey, C. E. Semler, J. B. Holt, *J. Am. Ceram. Soc.* **72**, 2318 (1990).
24. R. P. Elliott, *Constitution of Binary Alloys* (McGraw-Hill, New York, 1965), p. 233.
25. V. V. Aleksandrov and M. A. Korchagin, *Fiz. Goreniya Vzryva* **23**, 55 (1987).
26. Y. S. Touloukian, Ed., *Thermophysical Properties of High Temperature Solid Materials* (Macmillan, New York 1967), vol. 1, p. 704.
27. J. Wong, P. A. Waide, J. B. Holt, B. Rupp, E. M. Larson, in preparation.

28. We acknowledge experimental assistance from L. Fareria, J. Scrofani, G. Lamble, S. M. Heald, M. Wilt, and L. Summers. Technical discussions with F. W. Lytle, A. Larson, and L. Tanner are appreciated. This work is supported under the auspices of the U.S. Department of Energy (DOE) by the Lawrence Livermore National Laboratory under contract W-7405-ENG-48. We are also grateful for the support of DOE, Division of Materials Sciences, under contract DE-AS05-80-ER10742, for its role in the development and operation of Beam Line X-11 at the NSLS. The NSLS is supported by DOE, divisions of Materials Sciences and Chemical Sciences, under contract DE-AC02-76CH00016.

13 March 1990; accepted 21 June 1990

Rapid Determination of the Critical Temperature in Simulated Annealing Inversion

ATANU BASU AND L. NEIL FRAZER*

Knowledge of the critical temperature, T_*, the temperature at which a phase change occurs, greatly improves the efficiency of simulated annealing when used for optimization or inversion. A numerical method of accurately determining T_* in a relatively short computation time has been developed. This method is used to recover the seismic soundspeed profile from wavefield data, a problem in which cycle skipping causes many local minima of the energy function and the averaging of the medium by finite length waves results in many states with similar energies. Computations indicate that it is cost-effective to spend about 80 percent of the computing budget looking for T_* instead of annealing, and that in the course of finding T_* many states with energies near the global minimum will also be found. The a posteriori probability distribution of the solution has been constructed from trial solutions generated at T_*.

SIMULATED ANNEALING (SA) WAS INvented independently by Kirkpatrick, Gelatt, and Vecchi (*1*) and by Černy (*2*). SA makes use of the principle that for a system of particles having random configurations at a fixed temperature T the probability of finding the system in state j with energy E_j is given by the Gibbs distribution

$$g_j = \exp(-E_j/T)/Z \quad (1)$$

in which the partition function Z is given by a sum over all possible states

$$Z = \sum_i \exp(-E_i/T) \quad (2)$$

Hawaii Institute of Geophysics, University of Hawaii at Manoa, Honolulu, HI 90822.

*To whom correspondence should be addressed.

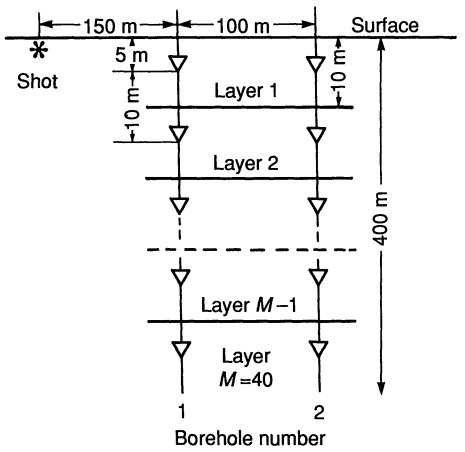

Fig. 1. Geometry of the model. Two boreholes are located 100 m apart with 40 geophones, spaced 10 m apart, in each borehole. The shot is located just beneath the surface 150 m to the left of borehole 1.

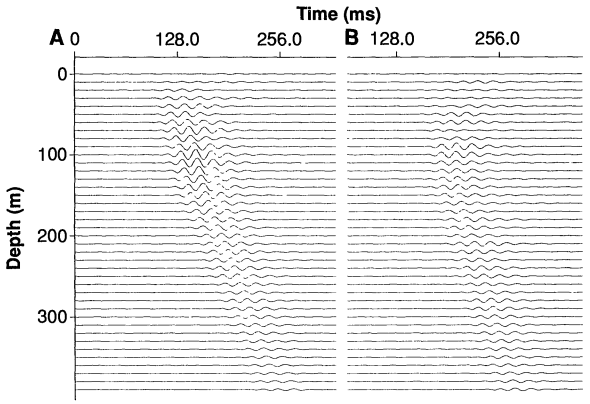

Fig. 2. (**A**) Wavefield observed in borehole 1; (**B**) wavefield observed in borehole 2.

When SA is used for optimization, the unknown parameters are regarded as particles, and the allowed values of a parameter correspond to the allowed states of its associated particle. The energy E in Eq. 1 is the cost function, and the temperature is lowered very slowly so that the system of particles eventually freezes into the global minimum of E. In our experiments, we used the heat bath algorithm (*3*). The Metropolis algorithm (*4*) is mathematically equivalent to the heat bath algorithm (*5*), but the heat bath algorithm may be more efficient than the Metropolis algorithm for inversion problems (*6*).

In the heat bath algorithm, each particle is visited in sequence. Visiting the ith particle, one fixes the states of other particles and calculates the system energy for each allowed state of particle i. These energies are used to generate a Gibbs distribution for particle i, from which a new state for particle i is chosen by sampling once. After each particle in the system has been visited once (this cycle is called a sweep), the temperature T is lowered by a small amount and then each particle is visited again. After many sweeps, the system will be in equilibrium at a low temperature, frozen into a global energy minimum. An M-particle system requires M random numbers per sweep.

The conditions under which SA can be proved to converge to the global minimum of E are often unacceptable because they require so much computer time. Thus, progress in SA depends on experiment as well as theory; experiments are generally used to select a cooling (annealing) schedule, a prescription for lowering T over time. A cooling schedule includes the starting temperature T_0, the rate of cooling, the amount of time to be spent at each temperature, and the time at which to stop. Theoretical approaches to the design of cooling schedules are given in (*7–9*). Rothman (*6*) found the global minimum in a seismic inversion problem by starting at a high temperature and then cooling slowly to just below T_*, the temperature at which a phase change occurs. He determined T_* by trial and error, that is, by repeated runs for different assumed values of T_*.

In our problem, theoretical cooling schedules (*7, 8*) gave poor results, and a trial and error determination of T_* required prohibitive amounts of computer time. Hence we developed a method to rapidly determine T_*. While finding T_* our method also finds many good solutions; thus, the issue of cooling schedules became far less important. We applied SA to an inverse problem (*10*), the problem of determining the soundspeed versus depth profile $c(z)$ of a layered earth from motions recorded in a borehole. As shown in Fig. 1, a seismic source is located 150 m away from the first of two boreholes and the resulting motion is recorded by geophones in both boreholes. In a stratified earth, the resulting data are identical to data recorded in a single borehole from two sources at different horizontal distances.

We chose this problem to experiment with SA, because the Green's functions necessary for its solution are more economical to compute than those of most other seismic inversion problems. All the other difficult characteristics of wavefield inversion problems are present, however, making SA inversion an appropriate method. Our soundspeed-depth profile has $M = 40$ layers, and each layer can have one of $N = 5$ possible soundspeeds, so the number of possible solutions is $N^M \approx 10^{26}$. Enormous computational time would be needed to examine this number of profiles even if geologically unlikely models are excluded. Furthermore, many geologically acceptable profiles differ greatly from each other, so traditional inversion methods that require linearization cause the final solution profile to be highly dependent on the starting profile. SA is independent of starting profile, and its efficiency relative to other methods increases rapidly with M, the number of unknowns. As our main purpose was to investigate SA, we used for the "observations" in the boreholes synthetic data computed by an exact method (*11*).

The wavefield observations (Fig. 2) in the first and second boreholes are $U_1(t, z)$ and $U_2(t, z)$, respectively, in which t is time and z is receiver depth. We calculate a theoretical borehole 2 data set $\tilde{U}_2$ using U_1 at all depths and an assumed soundspeed profile $c(z)$. This process is called migration. If the migrated data $\tilde{U}_2$ agree perfectly with the

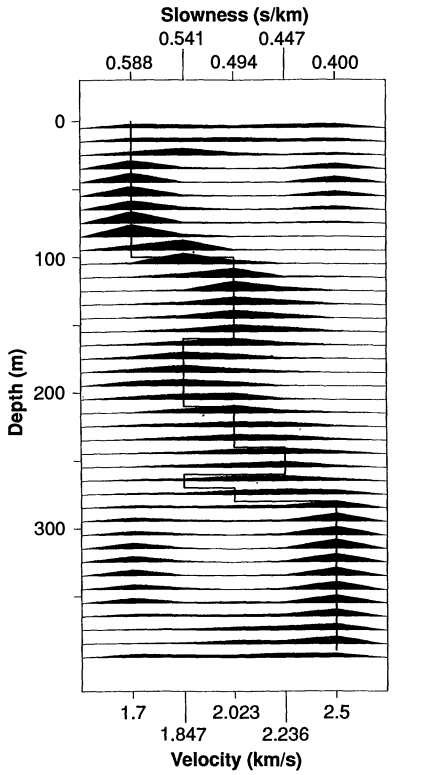

Fig. 3. A posteriori probability distributions (PPDs) for soundspeed at each depth. The true profile is indicated by the solid line. The PPDs were computed by a procedure called Gibbs-weighted graph-binning, explained in the text.

observed borehole 2 data U_2, then $c(z)$ is the true profile. We use SA to find that $c(z)$ which gives the best agreement between $\tilde{U}_2$ and U_2. For convenience, we assume a layered earth with the layer boundaries halfway between the receivers as shown in Fig. 1. Then $c(z)$ is piecewise constant and is represented as an array $\mathbf{c} = (c_1, \ldots, c_M)$ where $c_i = c(z_i)$ is the soundspeed of the ith layer. We restrict the soundspeed in each layer to five possible values, thus $c_i \in \{\gamma_1, \ldots, \gamma_5\}$.

Our algorithm for migration is a Kirchhoff-Fermat method similar to that used by Carter and Frazer (*12*). The $U_1(t, z)$ are weighted, time-shifted, and summed to generate $\tilde{U}_2(t, z)$ according to the relation

$$\tilde{U}_2(t, z_j) = \sum_k a_{jk} U_1(t - t_{jk}, z_k) + b_{jk} \hat{U}_1(t - t_{jk}, z_k) \quad (3)$$

in which $\hat{U}_1$ is the temporal Hilbert transform of U_1, a_{jk} and b_{jk} are weights, k is the depth index in borehole 1, j is the depth index in borehole 2, and t_{jk} is the time shift. The weights a_{jk} and b_{jk} are independent of $c(z)$ and depend only on the difference $j - k$ except near the tops and bottoms of the boreholes. The travel time t_{jk} is the integral of $1/c(z)$ along the straight line from depth z_k in borehole 1 to depth z_j in borehole 2.

Agreement of the zero-mean time series $\tilde{U}_2$ and U_2 is measured by the correlation

$$\varphi(\tilde{U}_2, U_2) = \frac{1}{N_Z} \sum_{j=1}^{N_Z} \left\{ \frac{\sum_{t=1}^{N_t} \tilde{U}_2(t, z_j) U_2(t, z_j)}{\left[\sum_{t=1}^{N_t} \tilde{U}_2(t, z_j)^2\right]^{1/2} \left[\sum_{t=1}^{N_t} U_2(t, z_j)^2\right]^{1/2}} \right\} \quad (4)$$

in which N_t is the number of points in each time series and N_Z is the number of receivers. The correlation would be 1.0 if the soundspeed profile used in migration were the true profile and our migration algorithm were perfect. In practice, our imperfect migration algorithm yields a correlation whose maximum approaches 0.92, a value that varies with the true profile. To apply SA, we define the energy E as the negative correlation, plus a small penalty term to discriminate against highly oscillatory profiles:

$$E(\mathbf{c}) = -\varphi(\tilde{U}_2, U_2) + \epsilon P(\mathbf{c}) \quad (5)$$

If we ignore the penalty term, $E \in [-1, 1]$. The penalty term is given by

$$P(\mathbf{c}) = \frac{\sum_{i=2}^{N_Z - 1} |1/c_{i+1} - 2/c_i + 1/c_{i-1}|}{2(N_Z - 2)(1/c_{\min} - 1/c_{\max})} \quad (6)$$

where $c_{\max}$ is the largest permitted soundspeed and $c_{\min}$ is the minimum permitted soundspeed. The maximum possible value of $P(\mathbf{c})$ is 1.0, realized only when $\mathbf{c}$ oscillates between $c_{\max}$ and $c_{\min}$ in successive layers. For most realistic profiles, $P(\mathbf{c})$ is less than 0.1. In the experiments presented below, the value of ϵ in Eq. 5 was fixed at 1.0.

The acoustic wavefields shown in Fig. 2 were used as observations in our numerical experiments. These observations had been synthesized elsewhere by an exact method based on the use of the true soundspeed profile indicated by the line in Fig. 3. As the wavelet of the seismic source was strongly peaked at 50 Hz, side lobes of the correlation function gave a high percentage of states with relatively low energies but inaccurate sound speed profiles. This is called cycle skipping.

To describe our method for determining T_* we first introduce the concept of a short run. A short run is a run at fixed temperature T that begins with a random soundspeed profile $\mathbf{c}_r$ and consists of 25 sweeps requiring a set $\mathbf{R}$ of $25M$ random numbers. At the end of each sweep, we save the energy E. The energies of the 25 sweeps in the short run are averaged to give $\bar{E}_{25} = \bar{E}_{25}(T, \mathbf{c}_r, \mathbf{R})$. We make other short runs at temperatures between 10^{-3} and 10^1, beginning with the same $\mathbf{c}_r$ and the same $\mathbf{R}$. As shown in Fig. 4A, these short runs give the graph of $-\bar{E}_{25}(T, \mathbf{c}_r, \mathbf{R})$ (solid line) versus $\log_{10} T$.

To reduce the dependence of $\bar{E}_{25}$ on $\mathbf{c}_r$ and $\mathbf{R}$, we make this series of runs five times with five different $\mathbf{c}_r$ and five different $\mathbf{R}$. The results are shown as solid lines in Fig. 4, A through E. The five different graphs of $\bar{E}_{25}(T, \mathbf{c}_r, \mathbf{R})$ versus $\log_{10} T$ are averaged to give the graph of $\bar{E}_{25}(T)$ shown in Fig. 4F: thus

$$\bar{E}_{25}(T) \approx \frac{1}{5} \sum_{\{\mathbf{c}_r, \mathbf{R}\}} \bar{E}_{25}(T, \mathbf{c}_r, \mathbf{R}) \quad (7)$$

We define T_* to be the temperature at which $-\bar{E}_{25}(T)$ attains its maximum. From Fig. 4F, $\log_{10} T_*$ was estimated as -2.0 ± 0.2. We refer to T_* as the critical temperature because in the short runs at $T = T_*$, E usually dropped sharply within 10 to 20 sweeps. To show the effect of the penalty function in Eq. 6, Fig. 4 includes the graph of $\bar{\varphi}_{25}(T)$ (dashed lines), computed at the same time as $-\bar{E}_{25}(T)$.

The curves in Fig. 4 are low at low T because the system is too cold to find its way out of the local energy minimum nearest to the starting model; they are low at high T because, at high T, high-E states are as acceptable as low-E states. The peak temperature T_* represents a balance point at which low-E states are preferred, but the system is warm enough to tunnel between such states.

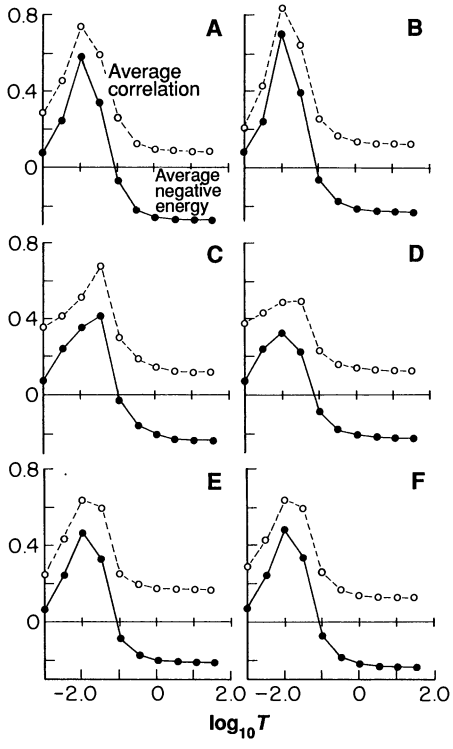

Fig. 4. Curves plotted in (**A**) show average correlation (dashed line) and average negative energy (solid line), for 25 sweeps at a fixed temperature. At each temperature, a 25-sweep run was made with the same set of $25M$ random numbers and the same random starting model. We computed the curves in (**B**), (**C**), (**D**), and (**E**) as for (A) but used different sets of $25M$ random numbers and different random starting models. The curves in (**F**) are the averages of the curves in (A) through (E). The temperature at the peak of the average energy curve in (F) is defined to be T_*.

We repeated the experiment described here for a variety of true soundspeed profiles, with similar results. We found that T_* is different for different true soundspeed profiles and that it also changes with the value of ϵ, the penalty weight in Eq. 5. Any change in the definition of E or any change in the data set $\{U_1, U_2\}$ changes T_*. This behavior is analogous to that of a melt whose freezing point is sensitive to small changes in the proportions of minor components.

We also explored alternative definitions of average short-run energy. For example, at each temperature, instead of making five runs with five sets of $25M$ random numbers, we made a single run with one set of $125M$ random numbers. The difference is that with five shorter runs the system is set to the starting model five times instead of once. The resulting graphs of $-\bar{E}(T)$ were higher than those in Fig. 4F, but the peak was at the same temperature. We obtained slightly smoother graphs for $\bar{E}(T)$ by using the same set of random numbers at each temperature rather than different sets at different tem-

peratures.

Once T_* had been found, it was no longer necessary to cool slowly from a high initial temperature. By starting at $T = 1.0$ and cooling to $T = T_*$ in 100 sweeps, then remaining at T_* for another 50 sweeps, we obtained profiles whose energies differed from the energy of the true profile by less than 5%. Below T_*, very slow cooling for several hundred sweeps gave profiles with energies less than 1% above the energy of the true profile. We found many low-E profiles while constructing Fig. 4.

In problems of the type considered here, the most important question is not what single profile fits the data best but rather what set of profiles fits the data well. The latter question is addressed by estimating the a posteriori probability distribution (PPD) for the soundspeed at each depth. Mathematically, the PPD for the c_i, the soundspeed at the ith depth, is given by

$$p(c_i|U_1, U_2) = \sum_{c_1} \sum_{c_2} \ldots \sum_{c_{i-1}} \sum_{c_{i+1}} \ldots \ldots \sum_{c_M} p(\mathbf{c}|U_1, U_2) \quad (8)$$

Numerically, we construct this PPD by the following recipe, which we call Gibbs-weighted graph-binning. Let A be the set of profiles found at $T = T_*$ during construction of Fig. 4 and let $B \subset A$ be those profiles in A for which $c_i = \gamma$, where γ is one of the allowed values for c_i. First, we estimate the partition function at $T = T_*$ by

$$Z_* \approx \sum_{\mathbf{c} \in A} \exp[-E(\mathbf{c})/T_*] \quad (9)$$

Then the PPD for $\mathbf{c}_i$ is estimated by

$$p(\mathbf{c}_i = \gamma|U_1, U_2) \approx \frac{1}{Z_*} \sum_{\mathbf{c} \in B} \exp[-E(\mathbf{c})/T_*] \quad (10)$$

The PPDs for our example are shown in Fig. 3. Note that Fig. 3 was constructed using only the 125 profiles found at $T = T_*$ during construction of Fig. 4, and that we constructed Fig. 4 by using only 10 (temperatures) × 25 (sweeps per temperature) × 5 = 1250 sweeps. The PPDs in Fig. 3 look the same for any T within our error bounds for T_*.

Another useful quantity is the mean profile at $T = T_*$, estimated by

$$\langle \mathbf{c} \rangle \approx \frac{1}{Z_*} \sum_{\mathbf{c} \in A} \mathbf{c} \exp[-E(\mathbf{c})/T_*] \quad (11)$$

The ith component of $\langle \mathbf{c} \rangle$ is the centroid of the PPD for $\mathbf{c}_i$. Figure 3 shows that $\langle \mathbf{c} \rangle$ is not as good an estimator of the true profile as is the profile whose ith component is the peak value of the ith PPD. For example, in Fig. 3 the PPDs between 300 m deep and 350 m deep have their peaks at the true profile, but their centroids are to the left of the true profile indicated by the thin line.

Our numerical experiments indicate that for SA optimization and inversion problems one should spend most of the sweep budget determining T_*. Then for optimization problems, the conventional slow cooling schedule should be replaced by a schedule with rapid cooling to T_*. The process of finding T_* gives all the information necessary to estimate the PPD, a quantity much more useful in inversion than the profile with lowest energy.

REFERENCES AND NOTES

1. S. Kirkpatrick *et al.*, *IBM Res. Rep. RC 9355* (1982); S. Kirkpatrick, C. D. Gelatt, Jr., M. P. Vecchi, *Science* **220**, 671 (1983).
2. V. Černy, *J. Optimization Theory Appl.* **45**, 41 (1985).
3. C. Rebbi, in *Applications of the Monte Carlo Method*, K. Binder, Ed. (Springer-Verlag, New York, 1984), pp. 277–298; M. Creutz, *Phys. Rev. D* **21**, 2308 (1980).
4. N. Metropolis *et al.*, *J. Chem. Phys.* **21**, 1087 (1953).
5. P. J. M. van Laarhoven and E. H. L. Aarts, *Simulated Annealing* (Reidel, Boston, 1987).
6. D. H. Rothman, *Geophysics* **50**, 2784 (1985); *ibid.* **51**, 332 (1986).
7. S. Geman and D. Geman, *IEEE Trans. Pattern Anal. Mach. Intell.* **6**, 721 (1984).
8. H. Szu and R. Hartley, *Phys. Lett. A* **122**, 157 (1987).
9. J. D. Nulton and P. Salamon, *Phys. Rev. A* **37**, 1351 (1988); I. Matsuba, *ibid.* **39**, 2635 (1989).
10. W. Menke, *Geophysical Data Analysis: Discrete Inverse Theory* (Academic Press, New York, 1984); A. Tarantola, *Inverse Problem Theory* (Elsevier, New York, 1987).
11. S. Mallick and L. N. Frazer, *Geophysics* **53**, 479 (1988).
12. J. A. Carter and L. N. Frazer, *ibid.* **49**, 46 (1984).

13. Supported by the U.S. Office of Naval Research and by American Chemical Society grant PRF-20029-AC2. Hawaii Institute of Geophysics contribution 2328.

18 April 1990; accepted 29 June 1990

Forecasting Damaging Earthquakes in the Central and Eastern United States

S. P. NISHENKO AND G. A. BOLLINGER

Analysis of seismograph network data, earthquake catalogs from 1727 to 1982, and paleoseismic data for the central and eastern United States indicate that the Poisson probability of a damaging earthquake (magnitude ≥ 6.0) occurring during the next 30 years is at a moderate to high level (0.4 to 0.6). When differences in seismic wave attenuation are taken into account, the central and eastern United States has approximately two-thirds the likelihood of California to produce an earthquake with comparable damage area and societal impact within the next 30 years.

SINCE 1727 THERE HAVE BEEN SEVEN earthquakes with magnitudes greater than m_b (body-wave magnitude) 6.0 in the central and eastern United States. The largest five of these events [1811 to 1812 New Madrid, Missouri; m_b 7.0, 7.1, 7.2, 7.3 (*1*); and 1886 Charleston, South Carolina; m_b 6.7 (*2*)] occurred during the 19th century. In the 95 years that have elapsed since the last damaging $m_b \geq 6.0$ earthquake (*3*), the central and eastern United States has undergone an era of rapid urban growth along with the development of nuclear power plants, energy distribution systems, large reservoirs, and transportation and communications networks. The observations that earthquakes have occurred in this region in the past and that they are capable of producing structural damage over larger areas than their counterparts of similar size in California raise the obvious question: What are the chances for the occurrence of another $m_b \geq 6.0$ earthquake in the region east of the Rocky Mountains during the next few decades? We define a damaging earthquake as having a $m_b > 6.0$ (seismic moment magnitude, $\mathbf{M} \geq 6.1$), and consider exposure windows for the next 10, 30, 50, and 100 years.

Earthquake hazard assessments are primarily based on average rates of earthquake occurrence. Although information about earthquake recurrence times is lacking for specific fault zones in the central and eastern United States, regional rates of seismic activity are commonly estimated for hazards and engineering purposes by application of the Gutenberg-Richter frequency-magnitude or B value relationship, $\log N_C = A - BM$, where N_C is the cumulative number of earthquakes greater than or equal to a particular magnitude, M. The constants, A and B, are determined primarily from the rates of occurrence of smaller magnitude earthquakes and are used to estimate the rates of occurrence of infrequent larger magnitude

S. P. Nishenko, National Earthquake Information Center, U.S. Geological Survey, Denver, CO 80225.
G. A. Bollinger, U.S. Geological Survey and Seismological Observatory, Virginia Polytechnic Institute and State University, Blacksburg, VA 24061.